Carcinogenesis vol.27 no.5 pp.925–935, 2006
doi:10.1093/carcin/bgi315
Advance Access publication December 16, 2005

Efficient execution of cell death in non-glycolytic cells requires the generation of ROS controlled by the activity of mitochondrial H^+-ATP synthase

Gema Santamaría[1,†], Marta Martínez-Diez[1,†], Isabel Fabregat[2] and José M.Cuezva[1,*]

[1]Departamento de Biología Molecular, Centro de Biología Molecular Severo Ochoa, Universidad Autónoma de Madrid, 28049 Madrid, Spain and [2]IDIBELL-Institut de Recerca Oncològica, 08907 L'Hospitalet, Barcelona, Spain

*To whom correspondence should be addressed at: Centro de Biología Molecular 'Severo Ochoa', Universidad Autónoma de Madrid, 28049 Madrid, Spain. Tel: 34 91 497 4866; Fax: 34 91 497 4799;
Email: jmcuezva@cbm.uam.es

There is a large body of clinical data documenting that most human carcinomas contain reduced levels of the catalytic subunit of the mitochondrial H^+-ATP synthase. In colon and lung cancer this alteration correlates with a poor patient prognosis. Furthermore, recent findings in colon cancer cells indicate that downregulation of the H^+-ATP synthase is linked to the resistance of the cells to chemotherapy. However, the mechanism by which the H^+-ATP synthase participates in cancer progression is unknown. In this work, we show that inhibitors of the H^+-ATP synthase delay staurosporine (STS)-induced cell death in liver cells that are dependent on oxidative phosphorylation for energy provision whereas it has no effect on glycolytic cells. Efficient execution of cell death requires the generation of reactive oxygen species (ROS) controlled by the activity of the H^+-ATP synthase in a process that is concurrent with the rapid disorganization of the cellular mitochondrial network. The generation of ROS after STS treatment is highly dependent on the mitochondrial membrane potential and most likely caused by reverse electron flow to Complex I. The generated ROS promote the carbonylation and covalent modification of cellular and mitochondrial proteins. Inhibition of the activity of the H^+-ATP synthase blunted ROS production prevented the oxidation of cellular proteins and the modification of mitochondrial proteins delaying the release of cytochrome *c* and the execution of cell death. The results in this work establish the downregulation of the H^+-ATP synthase, and thus of oxidative phosphorylation, as part of the molecular strategy adapted by cancer cells to avoid ROS-mediated cell death. Furthermore, the results provide a mechanistic explanation to understand chemotherapeutic resistance of cancer cells that rely on glycolysis as the main energy provision pathway.

Abbreviations: AIF, apoptosis inducing factor; Endo G, endonuclease G; FCCP, carbonyl cyanide *p*-trifluoromethoxy-phenylhydrazone; OL, oligomycin; PCD, programmed cell death; PDTC, pyrrolidine dithiocarbamate; pI, isoelectric point; ROS, reactive oxygen species; STS, staurosporine.

[†]These authors contributed equally to this work.

Introduction

Mitochondria play a central role in the physiology of higher eukaryotic cells. Genetic and/or epigenetic alterations that impact on mitochondrial functions are thus involved in the development of a vast array of human pathologies (1). The provision of metabolic energy by oxidative phosphorylation (2) and the execution of cell death (3–6) are two cellular functions of mitochondria involved in the progression of human diseases. However, recent findings indicate the molecular and function integration of cellular metabolism with apoptosis (7–10). In this regard, the requirement of oxidative phosphorylation for efficient execution of cell death is a matter of debate. For instance, some authors have suggested that cells devoid of mitochondrial DNA (ρ°), which are unable to carry on oxidative phosphorylation, undergo apoptosis as efficiently as their parental ρ^+ cells (11–13) whereas other authors suggested the opposite, i.e. the ρ° cells have a resistant apoptotic phenotype (14–16). Contributing to the same debate it has been reported that oligomycin (OL), a specific inhibitor of the H^+-ATP synthase, is a promoter (17,18) or an inhibitor (19,20) of apoptosis. In addition, the activity of oxidative phosphorylation has been shown to be required for Bax-induced toxicity in yeast cells (21). Indeed, genetic screens in yeast, aimed at the identification of genes that could confer a Bax-resistance phenotype, allowed the identification of a subunit of the mitochondrial H^+-ATP synthase critical for Bax-mediating killing of *Sacchromyces cerevisiae* (19). Moreover, Bax-mediated killing of the budding yeast has been shown to be strictly dependent upon select mitochondrial components such as the nuclear encoded β-subunit of the H^+-ATP synthase and mitochondrial genome-encoded proteins (22). More recently, a specific repression of the expression of the β-subunit of the H^+-ATP synthase has been documented in rat hepatocarcinomas (23) as well as in the tumor biopsies of liver, colon, kidney, lung, breast, gastric and esophageal cancer patients (24–26). These findings have been recently confirmed (27–29) and extended to other carcinomas (30). Remarkably, the expression level of the β-subunit of the H^+-ATP synthase in lung (26) and colon (24) cancer significantly correlated with the prognosis of the patients. Moreover, recent findings indicate that resistance to 5-fluorouracil treatment is linked to the downregulation of the H^+-ATP synthase in colon cancer cells (31). Reasoning that there are enough indications for the participation of the H^+-ATP synthase in the execution of cell death and in cancer progression, we undertook the following approach designed to characterize the mechanistic contribution of the mitochondrial H^+-ATP synthase in staurosporine (STS)-triggered cell death in liver cells. The results presented support that the activity of the H^+-ATP synthase and, thus, the dependence on oxidative phosphorylation for cellular ATP provision defines the susceptibility of a cell to execute reactive oxygen species (ROS)-dependent cell death by the mitochondrial geared pathway.

Materials and methods

Cell cultures and cell recovery

Rat liver clone 9 (C9) (32) and rat hepatoma AS30D and FAO cells (23) were grown as described previously. The C9 and FAO cells were recovered from the plates by trypsin treatment except for those needed for the analysis of caspase 3 activities in which case they were scraped off in PBS. For all the assays AS30D cells were recovered by centrifugation.

Mitochondrial membrane potential ($\Delta\Psi m$) and mitochondrial mass

The fluorescent $TMRM^+$ and NAO probes (Molecular Probes, Eugene, Oregon) were used to analyze $\Delta\Psi m$ (33) and mitochondrial mass by flow cytometry, respectively. Different concentrations of carbonyl cyanide *p*-trifluoromethoxy-phenylhydrazone (FCCP) (0–5 μM) were used to titrate $\Delta\Psi m$. The cellular fluorescence intensity was measured using a FACScan flow cytometer (Becton–Dickinson, San José, CA). For each analysis 10 000 events were recorded.

Determination of caspase 3 activity

After various treatments the cells were harvested and lysed at 4°C in 5 mM Tris/HCl, pH 8.0, 20 mM EDTA and 0.5% Triton X-100. For the determination of caspase 3 activities the fluorescent caspase 3 substrate Ac-DEVD-AMC was used (34). Fluorescence was measured in a Microplate Fluorescence Reader FL600 Luminiscence Spectrophotometer (PerkinElmer LS-50) ($\lambda_{excitation}$, 380 nm; $\lambda_{emission}$, 440 nm). Protein concentration in the cellular lysates was determined using the Bio-Rad protein assay kit.

Protein electrophoresis and western blot analysis

The cells were resuspended in a lysis buffer containing 25 mM Hepes, 2.5 mM EDTA, 0.1% Triton X-100, 1 mM PMSF and 5 μg/ml leupeptin. Cellular proteins were fractionated on SDS–12% PAGE and then transferred onto PVDF membranes (23). The primary monoclonal antibodies used were: anti-caspase 9 antibody (NeoMarkers, 1:1000), anti-green fluorescent protein (anti-GFP) antibody (Clontech, 1:1000) and anti-α-tubulin antibody (Sigma, 1:1000). The primary polyclonal antibodies used were: anti-caspase 3 antibody (D157, Cell Signaling, 1:500), anti-endonuclease G (anti-Endo G) antibody (ψProSci Incorporated, 2 μg/ml), anti-apoptosis inducing factor (anti-AIF) antibody (Oncogene, 2.5 μg/ml), anti-Bax antibody (Santa Cruz, 1:1000), anti-Bcl-X_L antibody (Santa Cruz, 1:1000) and anti-β-F1-ATPase antibody (24). Peroxidase-conjugated anti-mouse or anti-rabbit IgGs (Nordic Immunology, 1:3000) were used as secondary antibodies. The blots were revealed using the luminol electrochemiluminescence (ECL®) reagent (Amersham Pharmacia Biotech, Little Chalfont, UK).

Nuclear DNA staining

Control and treated C9 cells growing on coverslips were fixed with 4% paraformaldehyde in PBS and further permeabilized with methanol. Cell nuclei were stained using a 300 nM solution of 4,6-diamidino-2-phenylindole (Sigma). Coverslips were observed in a Leica DMIRB fluorescence microscope ($\lambda_{excitation}$, 358 nm; $\lambda_{emission}$, 461 nm). The percentage of fragmented nuclei was counted in twenty different fields per condition assayed.

Analysis of the cell cycle and nuclear DNA content by flow cytometry

The cells were treated as indicated, harvested and fixed in 70% ice-cold ethanol for at least 12 h at 4°C. Afterwards, cells were treated with RNase (100 μg/ml) for 30 min at 37°C. The ploidy determination of the cells was estimated by flow cytometric analysis after staining of DNA with propidium iodide. The DNA content per cell was then evaluated in a FACScan. For computer analysis only the signals from single cells were considered (10 000 cells/assay).

Determination of ATP

Approximately 2×10^6 cells were precipitated and extracted with 100 μl of a 6% perchloric acid solution. After centrifugation at 15 000 *g*, to remove cell debris, the resulting supernatants were neutralized with 2% KOH. The determination of the cellular concentration of ATP was carried out by standard enzymatic procedures.

Determination of mitochondrial width

The distribution and morphology of mitochondria in cells exposed to different conditions was analyzed in C9 cells stably expressing a variant of gfp (32) that is localized in the matrix of the organelle (Martínez-Diez *et al*., to be described elsewhere) using a Leica DMIRB fluorescence microscope equipped with a GFP excitation filter (Leica, Switzerland; BP 470/40).The mitochondrial transversal section (width) is the most constant dimension of the organelle and variations on this parameter reflect an alteration of the morphology of mitochondria. The determination of the mitochondrial width was carried out in digital images acquired at ×60 magnification with a Leica DC100 camera. For processing of digital images the Leica QWin software package was used (32). For every condition tested, the width of 100–200 mitochondria in at least 100 different cells was determined.

Immunofluorescence/confocal microscopy

Fluorescence and indirect immunofluorescence microscopy was performed on mitochondria-tagged gfp C9 cells after various treatments. Cells grown on coverslips were fixed with 4% paraformaldehyde in PBS. Afterwards, the coverslips were treated with a solution containing 0.1% Triton X-100 in PBS for 10 min to permeabilize the cells. Coverslips were then blocked in a PBS solution containing 0.1% Triton X-100 and 1% fetal calf serum for 10 min. Coverslips were incubated with mouse monoclonal anti-cytochrome *c* antibody (PharMigen, 1:200). After three PBS rinses, the cells were incubated for 45 min in the dark with a 1:1000 dilution of goat anti-rabbit or goat anti-mouse IgGs conjugated to Alexa 594. Nuclei were stained with the label ToPro3 (Molecular Probes). Cellular fluorescence was analyzed by confocal microscopy using a Bio-rad Radiance 2000 Zeiss Axiovert S100TV using the following excitation/emission wave lengths: green (498/516 nm), red (590/617 nm) and blue (642/661 nm). In another set of experiments, C9 cells treated as indicated were incubated with 1 μM acridine orange for 10 min at 37°C. Afterwards, the cells were washed twice with PBS and the fluorescence emission of the probe analyzed in a Leica DMIRB fluorescence microscope.

Determination of reactive oxygen species

The analysis of intracellular H_2O_2 production was performed using two different oxidation-sensitive probes, $DCFH_2$-DA and C-2938 (Molecular Probes, Eugene, Oregon) and methodologies. For $DCFH_2$-DA staining by fluorimetry we proceeded as described (34). For C-2938 staining, approximately 5×10^5 cells were resuspended in 300 μl of PBS and incubated 30 min at 37°C with 5 μM C-2938. Propidium iodide (1 μg/ml) was used to detect dead cells that were excluded from the analysis. Cells were analyzed in a FACScan. For each analysis 10 000 events were recorded.

Detection of protein carbonylation

The Oxyblot Oxidized Protein Detection kit (Chemicon International) was used to detect protein oxidation of cellular proteins after various treatments. Dinitrophenylhydrazine (DNPH) derivatization was carried out as indicated by the supplier on 20 μg of cellular protein. Protein samples were fractionated on SDS–12% PAGE and processed for western blotting. The antibodies used were rabbit anti-DNPH (1:150) and goat anti-rabbit IgGs (1:300). The blots were revealed using the ECL® reagent (Amersham Pharmacia Biotech, Little Chalfont, UK).

Two-dimensional (2D) gel electrophoresis

Analytical 2D gel electrophoresis was performed to fractionate mitochondria-tagged gfp C9 cellular proteins using the immobiline DryStrip Kit (Pharmacia-LKB). Briefly, gels were rehydrated in a solution containing 8 M urea, 0.5% (v/v) Triton X-100, 1.3 mM dithiothreitol and 0.005% (v/v) Pharmalyte 3–10. The first dimension separation (IEF) was performed in 110 × 3 mm polyacrylamide gels containing an immobilized pH 3–10 gradient, at 300 V for 1 h and 1400 V for 17 h at a constant temperature of 20°C. The second-dimension separation (SDS) was in 12.5% polyacrylamide gels (14 × 13 cm) at room temperature overnight. Equal amounts of protein (175 μg) derived from freeze-dried cellular extracts were resuspended in the rehydration solution and applied to the strips. After electrophoresis, the gels were either stained or processed for western blotting.

Online supplementary material

For live imaging presented in the supplementary video, mitochondria-tagged gfp C9 cells were grown on glass plates and live images in a Cell Observer Zeiss equipment were taken using a Zeiss Axiovert 200 inverted microscope with a Coolsnap FX CCD camera (Roper Scientific). Images were taken every 3 min for 30 frames with a ×40 objective and a gfp filter. The Metamorph 6.1r6 (Universal Imaging) program was used for image processing.

Results

The activity of the H^+-ATP synthase is required for efficient execution of cell death in C9 liver cells

Consistent with previous findings (19,20,35) we observed that 3 h pre-incubation of C9 cells with OL significantly delayed the cell-death response to STS as assessed both by the analysis of cell nuclei morphology (Figure 1A) and intracellular DNA content (Figure 1B). However, at 24 h after STS treatment the rates of cell death were not significantly affected in the cells

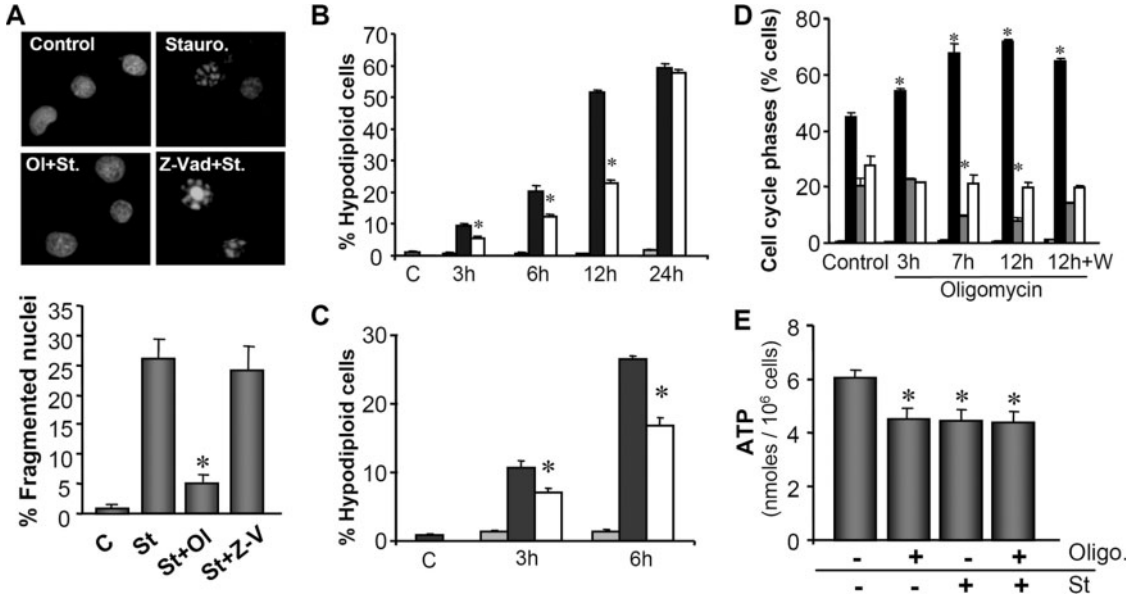

Fig. 1. Oligomycin delays STS-mediated cell death. C9 cells were treated as indicated. 1 μM STS (St), 6 μM OL (Ol), 20 μM z-VAD.fmk (Z-V) and 20 μM aurovertin B (Av) were used. (**A**) Assessment of nuclear DNA fragmentation by fluorescence microscopy at ×100 magnification and quantification of fragmented nuclei at 6 h after initiation of STS treatment. The results shown are the means ± SEM of four experiments. $^{*}P < 0.05$ when compared with STS-treated cells. (**B**) FACS analysis of the percentage of hypodiploid cells at various times after STS treatment. Gray bars, OL; closed bars, STS; and open bars, OL + STS. The results shown are the means ± SEM of five experiments. $^{*}P < 0.05$ when compared with STS-treated cells. (**C**) FACS analysis of the percentage of hypodiploid cells after treatment with aurovertin B. Gray bars, Av; closed bars, STS; and open bars, Av + STS. The results shown are the means ± SEM of six experiments. $^{*}P < 0.05$ when compared with STS-treated cells. (**D**) Cells were treated with OL for the indicated times and the percentage of cells in each of the cell cycle phases determined by flow cytometric analysis. In 12 h + W, cells were treated with OL for 12 h and maintained for additional 3 h in the absence of the drug before proceeding to the analysis of the cell cycle. (Closed bars, G_0/G_1; gray bars, S; and open bars, G_2/M.) The results shown are the means ± SEM of three experiments. $^{*}P < 0.05$ when compared with non-treated cells. (**E**) Determination of cellular ATP content. The results shown are the means ± SEM of four experiments. $^{*}P < 0.05$ when compared with non-treated cells.

treated with OL (Figure 1B). At short term, OL treatment was a stronger repressor of cell death than the caspase inhibitor z-Vad.fmk (Figure 1A). To confirm the specific role of the H^+-ATP synthase in the execution of cell death aurovertin B, a different inhibitor of the mitochondrial enzyme, was used. The results obtained revealed essentially the same findings as those obtained with OL (Figure 1C).

Liver C9 cells treated with OL were arrested at the G_0/G_1 phase of the cell cycle (Figure 1D) with significant reduction of cells in S-phase and accumulation of cells at G_0/G_1 as treatment with the drug persisted (Figure 1D). OL *per se* did not promote the induction of cell death in this cell line even after 12 h of treatment (Figure 1B and D). Removal of OL from the culture medium allowed the re-establishment of cell proliferation (Figure 1D). These results suggest that ATP produced by oxidative phosphorylation is required to enter into the S-phase of the cell cycle. Consistent with this finding, we observed that inhibition of the H^+-ATP synthase by OL promoted a significant ∼25% reduction in the cellular concentration of ATP (Figure 1E). However, the cellular concentration of ATP in OL-treated cells was not significantly different from that of cells treated with STS or with the combination of both drugs (Figure 1E).

Inhibition of other cellular ATPases enhanced STS-induced cell death

To exclude possible side effects of OL on other cellular ATPases we studied its effect on the subcellular compartmentalization and fluorescence emission of acridine orange. In normal cells, this fluorophore is trapped within acidic cellular granules (Figure 2). OL did not affect the subcellular

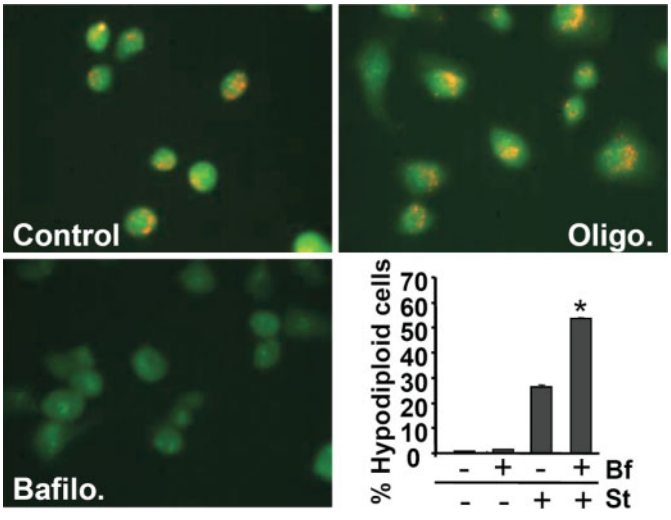

Fig. 2. Inhibition of other cellular ATPases enhanced STS-mediated cell death. C9 cells were treated as indicated. 1 μM STS (St), 6 μM OL (Oligo.) and 50 nM bafilomycin B1 (Bafilo/Bf) were used. C9 cells incubated with 1 μM acridine orange visualized by fluorescence microscopy. Cells are shown at ×40 magnification. The results illustrate the lack of effect of OL on other cellular ATPases. The histogram shows the FACS analysis of hypodiploid cells. Inhibition of non-mitochondrial ATPases by bafilomycin significantly increased STS-triggered cell death. The results shown are the means ± SEM of four experiments. $^{*}P < 0.05$ when compared with STS-treated cells.

distribution and fluorescence emission of acridine orange in C9 cells (Figure 2), suggesting the lack of effect of the inhibitor of the mitochondrial H^+-ATP synthase on the activity of other cellular ATPases. In contrast, bafilomycin B1, an

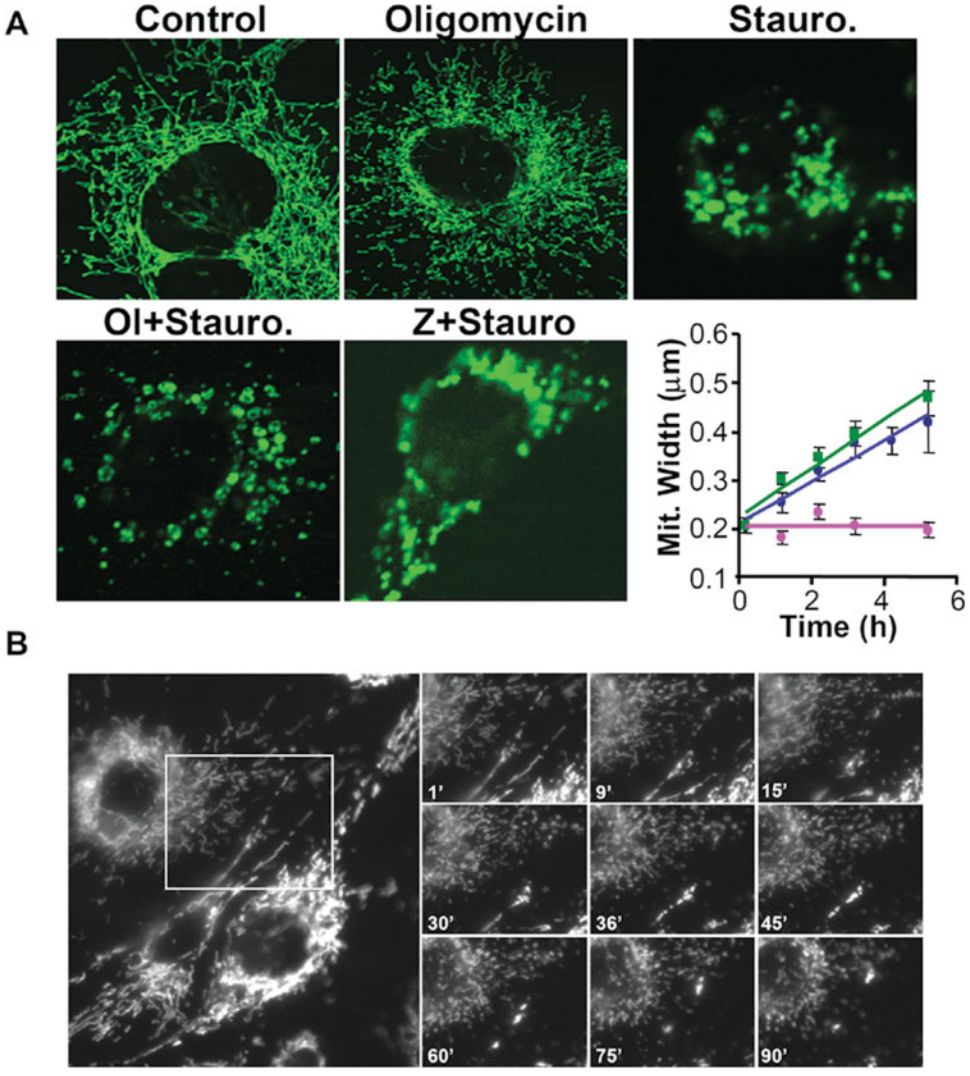

Fig. 3. Changes in cellular mitochondrial morphology after STS treatment are not influenced by OL. Mitochondria-tagged gfp C9 cells were treated as indicated and visualized by fluorescence microscopy. Aliquots of 1 μM STS (Stauro.), 6 μM OL (Ol.) and 20 μM z-VAD.fmk (Z) were used for treatments. (**A**) Typical cellular morphologies are shown for each condition at ×60 magnification. The plot shows the time-course changes in mitochondrial width recorded in OL (pink), STS (blue) and OL + STS (green) treated cells. The results shown are the means ± SEM of 100–200 determinations in at least 50 different cells. (**B**) Different time-frames of the movie (see supporting video 1) illustrate the rapid STS-induced changes on the mitochondrial network. Note that within the first 15 min thread-like mitochondria fission and are disorganized. Afterwards, fragmented mitochondria fusion into larger size organelles and move towards the nucleus.

inhibitor of cellular ATPases unrelated to the mitochondrial H^+-ATP synthase (36), promoted the loss of the red emission signal of acridine orange as a result of the alkalization of the cellular granules triggered by the inhibition of the ATPases present in these organelles (Figure 2). Moreover, and contrary to the results obtained with OL (Figure 1A and B), incubation of the cells with STS plus bafilomycin B1 promoted a high increase in cell death, to levels even higher than those obtained when the cells were incubated with STS alone (Figure 2). These results suggest that prevention of cell death by OL is unrelated to side-effects of the inhibitor of the mitochondrial H^+-ATP synthase on other cellular ATPases.

Inhibition of H^+-ATP synthase does not prevent the dismantling of mitochondrial reticulum after STS treatment

To visualize the possible effects of OL on mitochondrial morphology after STS treatment we used a stable C9 cell line expressing gfp in their mitochondria. Treatment of the cells with OL did not significantly affect the distribution and morphology of mitochondria in liver C9 cells (Figure 3A). In contrast, STS treatment promoted the rapid (<10 min) dismantling of the cellular mitochondrial network, the migration of fragmented mitochondria towards the cell nucleus and the subsequent fusion of mitochondria into larger size organelles (see video 1 in supplementary material and Figure 3A). Different time-frames of the movie illustrating the STS-mediated changes on the mitochondrial network are presented on Figure 3B. However, the effects of STS on mitochondrial morphology were not prevented by incubation of the cells with OL (Figure 3A) or with the caspase inhibitor z-Vad.fmk (Figure 3A).

Inhibition of H^+-ATP synthase delays the release of cytochrome c from mitochondria

Determination of the mitochondrial membrane potential ($\Delta\Psi m$) after priming the cells to death revealed an early

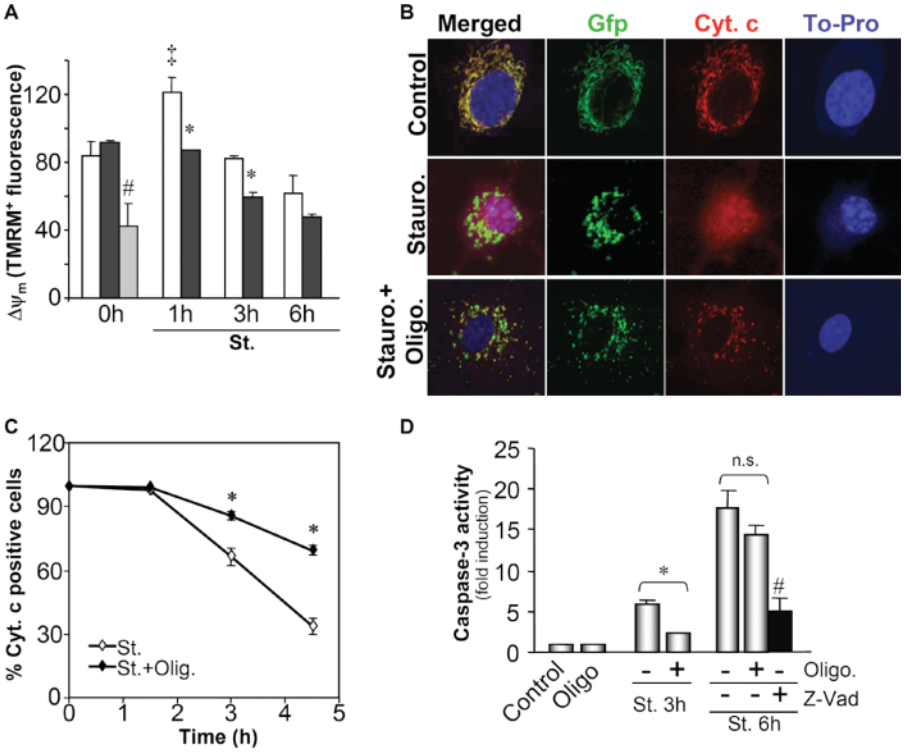

Fig. 4. The release of cytochrome *c* and activation of caspase 3 is delayed in OL-treated cells. Mitochondria-tagged gfp C9 cells were treated as indicated with none (Control) or 1 μM STS in the absence (Stauro.) or presence of 6 μM OL (Stauro. + Oligo.). (**A**) FACS determination of the mitochondrial membrane potential (ΔΨm) in STS (open bars) and STS + OL (closed bars) treated cells. ΔΨm was also assessed in C9 cells treated for 30 min with 50 μM of the mitochondrial uncoupler FCCP (Gray bar). The results shown are the means ± SEM of four to six experiments. $^*P < 0.05$ when compared with STS-treated cells. ‡ and #, $P < 0.05$ when compared with 0 h non-treated cells. (**B** and **C**) At various times after initiation of the STS treatment the cells were analyzed by immunofluorescence microscopy using anti-cytochrome *c* antibody. Nuclear DNA was stained with To-Pro. Typical morphologies of the cells at 3 h after STS-treatment are shown (**B**) for each condition at ×60 magnification. Quantification of the percentage of cytochorme *c* positive cells (**C**). The results are the means ± SEM of three experiments. $^*P < 0.05$ when compared with STS-treated cells. (**D**) Time course of the effect of OL on the activation of caspase 3 activity and inhibition of caspase 3 activation after 1 h pre-incubation of C9 cells with 20 μM z-Vad.fmk (closed bar). The results shown are the means ± SEM of four experiments. * and #, $P < 0.05$ when compared with 3 or 6 h STS-treated cells, respectively.

(1 h) increase in TMRM$^+$ fluorescence in STS treated cells (Figure 4A). Contrary to this finding, we observed no significant changes in NAO fluorescence after STS treatment of the cells (data not shown). The increase in TMRM$^+$ fluorescence triggered by STS was obliterated in the presence of OL (Figure 4A). Thereafter, ΔΨm declined in both STS and STS + OL treated cells (Figure 4A). It should be noted that using the pH sensitive BCECF-AM fluorescent probe we were unable to detect acidification of the cell cytoplasm in response to STS treatment during the early stage (first 3 h) of cell death (data not shown).

The release of cytochrome *c* from mitochondria-tagged gfp C9 liver cells was studied in response to treatment of the cells with STS and STS + OL (Figure 4B and C). Figure 4B illustrates the STS-induced morphological changes on mitochondria, the release of cytochrome *c* and the fragmentation of nuclear DNA in C9 cells treated with STS for 3 h. Treatment of the cells with OL was unable to prevent the changes on mitochondrial morphology but prevented STS-induced nuclear DNA fragmentation (Figure 4B, 1A and B) and significantly affected the release of cytochrome *c* from mitochondria (Figure 4B and C). In agreement with this last observation we noted that the activation of caspase 3 in response to STS treatment was significantly delayed in the presence of OL (Figure 4D) although this effect was not significant at longer times of incubation (Figure 4D). The mitochondrial release of cytochrome *c* was initiated after 90 min incubation of the cells with STS (Figure 4C), a time when morphological changes on the mitochondrial network had already occurred (Figure 3B and movie 1 in supplementary material). It should be noted that inhibition of the mitochondrial permeability transition pore with CsA did not prevent the release of cytochrome *c* from mitochondria and the induction of cell death after STS treatment (data not shown).

The H$^+$-ATP synthase controls the production of ROS after STS treatment

STS treatment of liver cells promoted a rapid (maximum production at ∼90 min) and significant increase in the production of H_2O_2 as assessed by two different methods and fluorescent probes (Figure 5A and B). Incubation of liver cells with rotenone, an inhibitor of Site I of the respiratory chain, blocked the STS-mediated increase in H_2O_2 production (Figure 5A). Interestingly, OL also abolished the STS-mediated increase in ROS production (Figure 5A and B). Consistent with a role for the generated ROS in signaling the execution of cell death we observed that STS-mediated cell death was also significantly reduced in rotenone-treated C9 cells (∼50%, $P < 0.005$, data not shown). Moreover, titration of ΔΨm with increasing concentrations of FCCP indicated a dose-dependent reduction of H_2O_2 production as ΔΨm declines (Figure 5C).

Limiting ROS availability after STS treatment delays the release of cytochrome c from mitochondria and the execution of cell death

To establish a link between mitochondrial ROS production and the execution of cell death the effects of two antioxidants were studied. α-Tocopherol is not able to quench mitochondrial ROS production and consistently it did not prevent ROS production and cell death triggered by STS (data not shown). In contrast, pyrrolidine dithiocarbamate (PDTC), a well characterized antioxidant in liver cells, partially quenched ROS production after STS treatment (Figure 5D) and blunted the STS-mediated cell death in C9 cells (Figure 5E). Moreover, a significant delay in the release of cytochrome *c* was observed in PDTC-treated cells after STS treatment (Figure 5F). Consistent with this finding, we observed that PDTC treatment arrested the STS-induced activation of caspase 3 (Figure 5G).

The H^+-ATP synthase controls the extent of oxidative modification of cellular proteins

One of the cellular targets of the toxic oxygen radicals is the covalent modification of proteins. Treatment of the cells with STS promoted a significant increase in the carbonylation of some cellular proteins (Figure 6A). Remarkably, incubation of the cells with OL prevented the STS-triggered oxidation of the proteins (Figure 6A). Likewise, the covalent modification of proteins could be tracked by changes in their isoelectric point (pI), as revealed by fractionation of cellular proteins on 2D-gels. Analysis of AIF in liver C9 cells treated with STS revealed that a large fraction of the protein experienced a significant acidic shift in its pI when compared with non-treated C9 cells (Figure 6B). Similar findings were obtained for Endo G (Figure 6B). OL treatment prevented the STS-mediated shift in the pI of AIF and Endo G (Figure 6B). It should be noted that the covalent modification of mitochondrial proteins after STS treatment is non-selective because it also affected the ectopically expressed gfp, an effect that was also partially prevented by OL (note the tailing in pI of the acidic form of gfp in Figure 6B). However, and in the specific case of gfp, OL *per se* also affected the pI of the expressed protein (see the basic gfp form in Figure 6B), suggesting the participation of additional factors in the modification of this protein.

The cellular dependence on oxidative phosphorylation determines the contribution of the H^+-ATP synthase to the execution of cell death. We next studied the contribution of the mitochondrial H^+-ATP synthase in the cell death response to STS in two hepatoma cell lines, FAO and AS30D, that differ substantially in their energetic phenotype [(23) and see references therein]. The FAO hepatoma has a differentiated phenotype qualitatively resembling that of the normal hepatocyte whereas the AS30D hepatoma has a poorly differentiated phenotype. Incubation of AS30D cells with OL did not affect the cellular concentration of ATP (Figure 7A), a finding that is consistent with the lack of dependence on oxidative phosphorylation for energy provision in this highly glycolytic cell line. Likewise, STS or the combination of STS plus OL treatment to AS30D cells did not affect the cellular concentration of ATP (Figure 7A). Analysis of cell death response to STS treatment in AS30D cells revealed that this hepatoma is highly resistant to the death stimulus because we observed no increase in the number of dying cells after 6 h treatment with the drug (data not shown). In agreement with the negligible contribution of the bioenergetic function of mitochondria to cellular energy

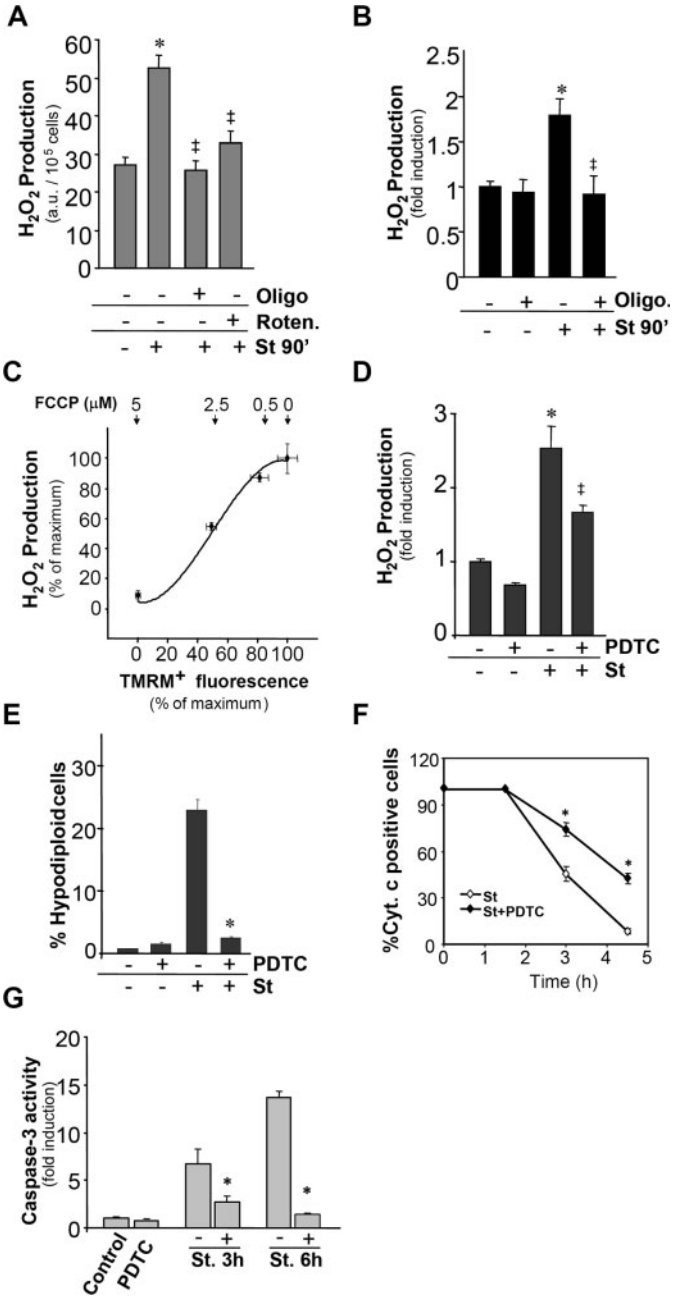

Fig. 5. The activity of the H^+-ATP synthase controls the generation of ROS after STS treatment. Liver C9 cells and/or mitochondria-tagged gfp C9 cells were treated as indicated. 1 μM STS (St), 6 μM OL (Oligo.), 2 μM rotenone (Roten) and 10 μM pyrrolidine dithiocarbamate (PDTC) were used for the treatments. (**A**) Fluorimetric determination of the generated H_2O_2 at 90 min after initiation of the STS treatment. The results shown are the means ± SEM of five experiments. * and ‡, $P < 0.05$ when compared with non-treated cells and STS-treated cells, respectively. (**B–D**) FACS determination of the generated H_2O_2 in OL-treated (**B**), FCCP (0–5 μM) uncoupled (**C**) and PDTC-treated (**D**) cells. The results shown are the means ± SEM of three, seven and seven experiments, respectively. * and ‡, $P < 0.05$ when compared with non-treated and STS-treated cells, respectively. (**E**) FACS analysis of hypodiploid cells in PDTC-treated cells. The results shown are the means ± SEM of six experiments. *$P < 0.05$ when compared with STS-treated cells. (**F**) At various times after initiation of the STS treatment mitochondria-tagged gfp C9 cells were analyzed by immunofluorescence microscopy and the percentage of cytochrome *c* positive cells quantified. The results are the means ± SEM of three experiments. *$P < 0.05$ when compared with STS-treated cells. (**G**) Time course of the effect of PDTC on the activation of caspase 3 after STS-treatment. The results shown are the means ± SEM of four experiments. *$P < 0.05$ when compared with STS-treated cells.

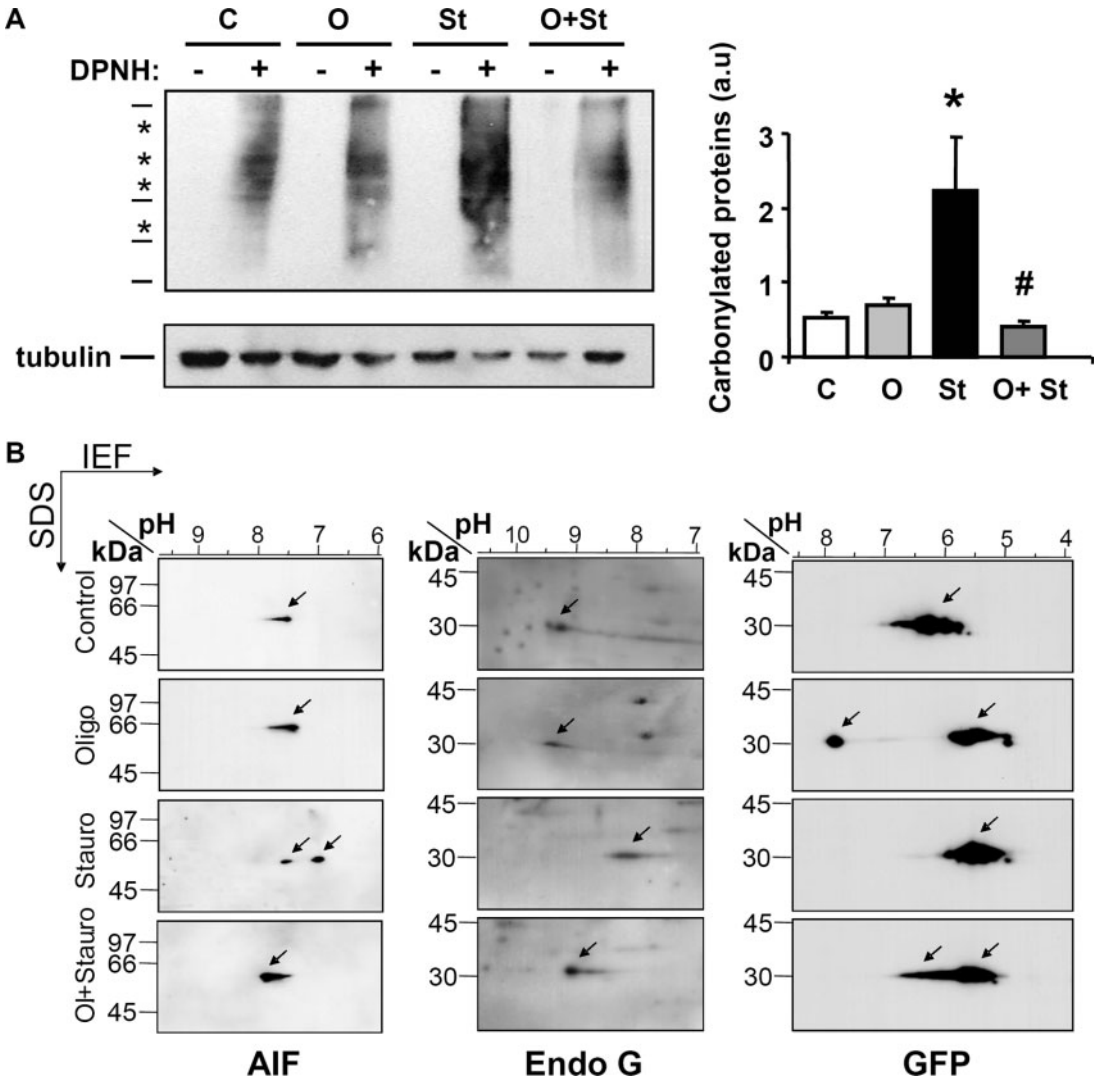

Fig. 6. The activity of the H^+-ATP synthase controls oxidative damage of cellular proteins. (**A**) C9 cells were treated as previously indicated. Cellular proteins (20 μg) were derivatizated in the absence (−) or presence (+) of DPNH and processed for the identification of protein carbonyls. Protein loading of the samples was verified by western blotting with anti-tubulin antibody. Molecular mass markers (97, 66, 45 and 30 kDa) are indicated to the left. The asterisks to the left of the gel identified the four proteins used for the quantification of protein carbonylation in response to the various treatments. A representative blot of three different experiments is shown. The results shown are the means ± SEM of three experiments. * and #, $P < 0.05$ when compared with control and STS-treated cells, respectively. (**B**) Mitochondria-tagged gfp C9 cells were treated as indicated. 1 μM STS (St) and 6 μM OL (Oligo.) were used for the treatments. Cellular proteins were fractionated after the indicated treatments on 2D-gels and AIF, Endo G and gfp visualized by western blot. Representative blots of three different experiments are shown. Arrowheads denote changes in the pI of the proteins.

provision in AS30D cells (Figure 7A), we observed no differences in ROS production after treatment of the cells with STS or with STS plus OL (Figure 7B).

In contrast, incubation of FAO cells with OL promoted a significant 3-fold decrease in the cellular content of ATP (Figure 7C), strongly suggesting that these cells largely depend on oxidative phosphorylation for cellular ATP provision. STS treatment also reduced the cellular ATP levels of FAO cells although not at a lesser extent than OL (Figure 7C). Contrary to the findings in AS30D cells, treatment of FAO cells with STS triggered the activation of cell death (Figure 7D). In agreement with the results found in C9 cells (Figure 1A and 4D), the caspase inhibitor z-Vad.fmk abrogated caspase 3 activation in FAO cells (Figure 7D), although it could only reduce partially the extent of cell death (Figure 7D). In addition, OL was as effective as z-Vad.fmk in preventing cell death in these cells (Figure 7D), indicating a relevant role for the H^+-ATP synthase in the execution of cell death in FAO cells. STS treatment of FAO cells also promoted a rapid (maximum production at ∼30 min) and significant increase in H_2O_2 production (Figure 7E). It should be noted that both the relative cellular production and time scale of H_2O_2 production after STS treatment were much more intense and rapid in FAO than in C9 cells (compare Figure 7E versus 5A and B for FAO and C9, respectively). Incubation of FAO cells with rotenone also blocked STS-mediated increase in H_2O_2 production ($P < 0.05$, data not shown). Consistent with the role of the H^+-ATP synthase in controlling the generation of ROS after STS treatment we found that OL significantly reduced H_2O_2 production in STS-treated FAO cells (Figure 7E). However, whereas in C9 cells OL completely blocked ROS production (Figure 5A and B), it was only able to reduce ROS production in FAO cells (Figure 7E), suggesting the existence of alternative pathways of ROS generation in this cell line.

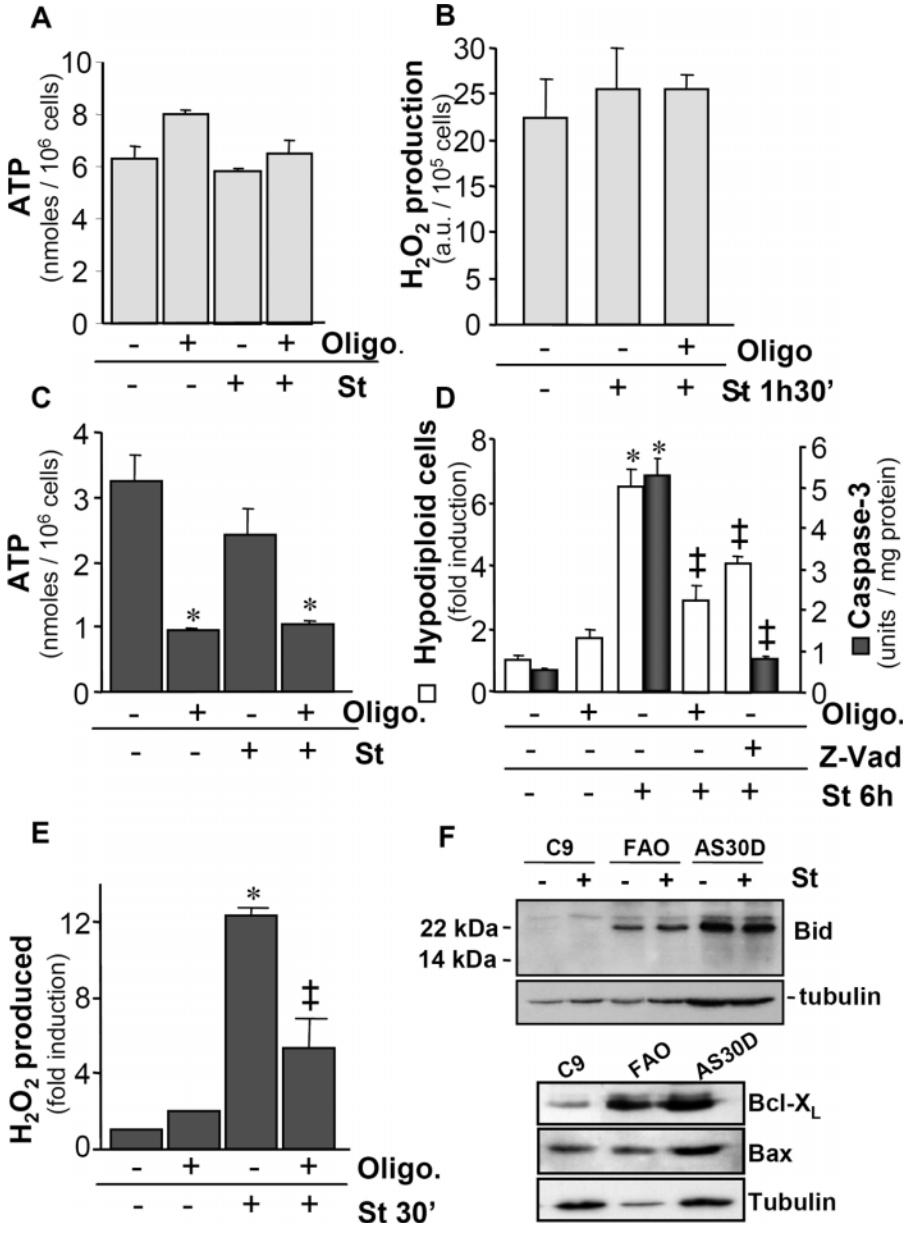

Fig. 7. Role of oxidative phosphorylation in STS-triggered cell death in hepatoma cells. AS30D and FAO hepatoma cells were treated as indicated with 1 μM STS. 6 μM OL was used for treatments. (**A**) Determination of cellular ATP content in AS30D cells after 6 h treatment with STS. The results shown are the means ± SEM of four experiments. (**B**) Fluorimetric determination of the generated H_2O_2 at 90 min after initiation of the STS treatment in AS30D cells. The results shown are the means ± SEM of three experiments. (**C**) Determination of cellular ATP content in FAO cells. The results shown are the means ± SEM of four experiments. $^*P < 0.05$ when compared with non-treated cells. (**D**) FACS analysis of hypodiploid cells (open bars) and determination of caspase 3 activity (closed bars) in FAO cells treated for 6 h with STS. 20 μM z-Vad.fmk was used as indicated. The results are the means ± SEM of three (cell death) and four (caspase 3) experiments. * and ‡, $P < 0.05$ when compared with non-treated and STS-treated cells, respectively. (**E**) FACS determination of the generated H_2O_2 at 30 min after initiation of the STS treatment in FAO cells. The results shown are the means ± SEM of three experiments. * and ‡, $P < 0.05$ when compared with non-treated and STS-treated cells, respectively. (**F**) Proteins from C9, FAO and AS30D cells were fractionated by SDS–PAGE and the putative processing of Bid analyzed by western blot after 6 h treatment with STS. The cellular expression of Bcl-X_L and Bax were also analyzed in these cells and expressed relative to the signal of tubulin.

Finally, to exclude the possibility that STS could also trigger cell death of the cell lines analyzed in this study (C9, FAO and AS30D) through the extrinsic pathway we analyzed the expression of Bid and truncated form of Bid in response to STS treatment. The results (Figure 7F) revealed an absence of Bid expression in C9 cells or of Bid processing in FAO and AS30D cells, suggesting that the cell death response to STS treatment in the C9 and FAO cells is primarily executed via the mitochondrial pathway. In addition, the relative cellular expression of Bax and Bcl-X_L were analyzed in C9, FAO and AS30D cells (Bcl-2 is not expressed in these cell lines). The results showed that the apoptotic potential of these cells, as assessed by the ratio of the pro-apoptotic Bax to the anti-apoptotic Bcl-X_L, was 4-fold and 8-fold higher in C9 cells than in FAO and AS30D cells, respectively (Figure 7F).

Discussion

Cells can engage in several programmed cell death (PCD) pathways in response to a death stimulus (6). In this study,

we have analyzed the cell death response to STS in liver cells that have a differential dependence on oxidative phosphorylation for cellular energy provision. The results indicate that the cell death response to STS differs significantly depending upon the relative activity of the mitochondrial pathway for the provision of metabolic energy. It appears that the H^+-ATP synthase is a key component of PCD because its activity is involved in the generation of ROS, a death signal that is generated in the early induction phase of PCD that is required for efficient execution of cell death (6,37,38). The generated ROS are further responsible for the oxidation and covalent modification of mitochondrial constituents facilitating in this way the release of apoptogenic molecules from the mitochondria that will effectively swamp the cells into death. Within this scenario, the cell death response triggered by STS in STS-sensitive liver cells has features of PCD executed both by apoptosis and caspase-independent cell death pathways, being the activity of the H^+-ATP synthase required in both pathways. It is unlikely that necrosis, triggered by ATP depletion of the cell, plays a role in STS-induced cell death in FAO and C9 cells. In fact, OL treatment induced a reduction in cellular ATP concentrations even larger (FAO cells) or at least similar (C9 cells) to that observed in STS-treated cells. However, in both cell lines OL treatment prevented cell death. These results are in agreement with a similar recent observation in MOLT-3 cells (39).

Molecular constituents that are involved in the regulation of the morphology of mitochondria play an important role in controlling the execution of cell death (40–42), although it appears that the contribution of such changes during apoptosis could depend on the nature of the death-inducing signal (43). A very early event after STS treatment is the dismantling of the cellular mitochondrial reticulum into punctiform organelles. We show here that OL is unable to prevent the alteration of the cellular mitochondrial reticulum after STS treatment. However, OL effectively delays the release of cytochrome *c* and the execution of cell death in response to STS, suggesting that the dismantling of the mitochondrial network is not sufficient to commit the cells to death and that the H^+-ATP synthase participates in the regulation of PCD downstream this event.

As previously shown by others (35,44), we observed that STS promoted an early increase in $TMRM^+$ retention in the mitochondria consistent with an increase in $\Delta\Psi m$ brought about by the inhibition of cellular respiration (45). Increased $TMRM^+$ retention may be due to a true increase in $\Delta\Psi m$ or to the apparent increase in mitochondrial volume that occurs early after STS addition (see Figure 3A). The findings that NAO fluorescence did not reveal significant changes after STS treatment (data not shown) and that OL + STS treatment to the cells caused similar changes on mitochondrial morphology to that of STS alone (see Figure 3A) but abrogated the increase in $TMRM^+$ retention (see Figure 4A) indicate a true increase in $\Delta\Psi m$ after STS treatment. It has been described that upon inhibition of mitochondrial respiration ATP generated by glycolysis supports $\Delta\Psi m$ (35,46–48). In this situation, the H^+-ATP synthase is forced to hydrolyze ATP generating matrix ADP^{3-} that would be exchanged with cytosolic ATP^{4-} generated by glycolysis. The electrogenic exchange of the nucleotides by adenine nucleotide translocase and the ATP-supported proton pumping activity of the ATPase are both likely to contribute to the maintenance of a high $\Delta\Psi m$ in the early phase after STS treatment (35,46–48). In fact, inhibition of the ATPase activity with OL prevented $\Delta\Psi m$ hyperpolarization after STS treatment. It is well established that ROS production by mitochondria is highly dependent on the proton motive force (49,50). We have observed that ROS production after STS treatment was dose-dependently inhibited by titration of $\Delta\Psi m$ with the uncoupler FCCP. Furthermore, ROS production after STS treatment was abolished in the presence of the inhibitor rotenone, consistent with ROS being produced in this situation owing to reverse transport of electrons from Complex II-linked respiratory substrates into Complex I [(50,51) and references therein]. Consistently, inhibition of the ATPase-supported high $\Delta\Psi m$ with OL suppressed ROS production.

Our results suggest that the ATPase-supported high $\Delta\Psi m$ induced by STS and the subsequent generation of ROS precede the release of cytochrome *c* from mitochondria. In fact, blocking the increase in $\Delta\Psi m$ by OL treatment prevented ROS generation, attenuated cytochrome *c* release and the activation of caspase 3, delaying the execution of PCD. Likewise, quenching of the generated ROS by PDTC treatment attenuated cytochrome *c* release and the execution of cell death, although we cannot exclude that PDTC might have additional effects on caspases (52), because caspase 3 activation and DNA fragmentation are completely blocked with this treatment. These findings support that the generated ROS are not an epiphenomenon of PCD but rather a required signal (53) for the efficient execution of cell death in oxidative phosphorylation-dependent (FAO and C9) cells. It has been suggested that reverse functioning of the H^+-ATP synthase contributes to cytoplasm acidification, as determined by changes in the fluorescence emission of a mitochondrial targeted pH-sensitive gfp probe (35). In our case, we were unable to detect significant acidification of the cytoplasm at early stages of PCD after STS treatment (data not shown). However, we did observe that mitochondrial-targeted gfp suffers ROS-mediated covalent modifications in response to STS treatment that might have affected the fluorescence spectrum of the pH-sensitive probe used in that study (35).

ROS are known to promote oxidative damage of cellular constituents (DNA, lipids and proteins) as well as alterations in the signal transduction pathways that control the expression of genes required to execute cell death (52,54). More recently, the diminished production of ROS observed in the non-cleavable p75 mutant of Complex I has also been associated with the maintenance of plasma membrane integrity and the externalization of phosphatidylserine (55). Consistent with a role for ROS in PCD, we illustrate here that the generated ROS after STS treatment promote the carbonylation of cellular proteins as well as covalent modifications of mitochondrial proteins. Remarkably, these modifications are prevented by inhibition of ROS production with OL, strongly supporting the role of the activity of the H^+-ATP synthase in controlling the extent of oxidative modification of mitochondrial constituents. Although the results in this study illustrate the rapid ROS-mediated covalent modification of AIF and Endo G, they do not necessarily imply that such changes are required for the cell death activity of these molecules. In fact, the apoptotic activity of AIF has been shown to be independent of such changes (56). Rather, we speculate that the extent of non-specific ROS-mediated modifications of mitochondrial constituents (illustrated on the ectopically expressed gfp) could represent a critical point of regulation of the mitochondria-geared PCD pathway because it could define the threshold value of irreversible damage of the mitochondria

and the set-point for the release of the mitochondrial arsenal that controls PCD.

Interestingly, our results indicate that the cell death response to STS differs significantly depending upon the relative contribution of mitochondrial oxidative phosphorylation to the provision of metabolic energy in the cell. In this regard, FAO, C9 and AS30D cells could, respectively, represent liver cell types that rely highly, moderately and not at all on mitochondrial oxidative phosphorylation for cellular energy provision as assessed by the effect of OL on their respective cellular ATP concentrations. While the FAO and C9 cells display a phenotype sensitive to the drug, the AS30D cells are resistant to the cell death stimulus. Consistently, the inhibition of the H^+-ATP synthase activity by OL attenuated the execution of apoptosis in FAO and C9 cells. Overall, these findings are in agreement with previous reports that described the importance of an efficient oxidative phosphorylation for the execution of apoptosis (14–16,21,35) and with the role of the H^+-ATP synthase in apoptotic cell death (19,20,22). Furthermore, our data suggest that the controversial findings in the literature regarding the requirement or not of oxidative phosphorylation for efficient execution of apoptosis could arise as a result of bioenergetic differences of the cellular types that have been studied. Nonetheless, it should be noted that the cell death response to STS could also be modulated by additional cellular factors. In this regard, the higher Bax/Bcl-X_L ratio found in C9 than in FAO cells might contribute to the higher total apoptosis observed in C9 cells after STS treatment.

The generation of ROS is a physiological process that depends on the cellular activity of mitochondrial respiration, determining the lifespan of cells and organisms (57). On the other hand, and perhaps unexpectedly, glycolysis, the alternative energy producing pathway of the cell, is also integrated with apoptosis (7–9). In this regard, we suggest that cells that rely heavily on glycolysis for energy production, such as the AS30D hepatoma, display an apoptotic resistant phenotype similar to ρ° cells (14–16) because ROS signaling after chemotherapeutic targeting of the mitochondria is blunted. In contrast, cells that depend on oxidative phosphorylation for ATP provision experience PCD via ROS signaling. Therefore, it is not surprising that the expression of the H^+-ATP synthase, and perhaps of other OXPHOS complexes, is downregulated in most human tumors whereas the expression of some glycolytic markers shows just the opposite trend (24–26). This situation provides the cancer cell with an advantageous bioenergetic phenotype because the potential for ROS production is diminished, oxidative damage to cellular constituents would be reduced and the threshold for PCD induction will be higher, while glycolytic metabolism could support the energetic demand that allows cellular proliferation and tumor expansion.

Supplementary material

Supplementary material can be found at: http://www.carcin.oxfordjournals.org/.

Acknowledgements

We thank Mulchand S.Patel (State University of New York), Jorgina Satrústegui (CBMSO) and Juan M.Zapata (The Burnham Institute) for comments and helpful discussions. We also thank Carlos Sánchez for his expert guidance and help with video experiments. Margarita Chamorro, Francisco Murillo, Blanca Herrera and Miguel Murillo are acknowledged for excellent technical assistance. G.S. and M.M.-D. were supported by pre-doctoral fellowships from the Ministerio de Ciencia y Tecnología. This work was supported by grants from the Ministerio de Sanidad y Consumo (PI041255), Comunidad de Madrid (SAL/0026/2004) and Ministerio de Ciencia y Tecnología (BMC2001-0710). The CBMSO receives an institutional grant from Fundación Ramón Areces.

Conflict of Interest Statement: None declared.

References

1. Wallace,D.C. (1999) Mitochondrial diseases in man and mouse. *Science*, **283**, 1482–1488.
2. Boyer,P.D. (1997) The ATP synthase—a splendid molecular machine. *Annu. Rev. Biochem.*, **66**, 717–749.
3. Ferri,K.F. and Kroemer,G. (2001) Organelle-specific initiation of cell death pathways. *Nat. Cell. Biol.*, **3**, E255–263.
4. Wang,X. (2001) The expanding role of mitochondria in apoptosis. *Genes Dev.*, **15**, 2922–2933.
5. Reed,J.C. (1999) Mechanisms of apoptosis avoidance in cancer. *Curr. Opin. Oncol.*, **11**, 68–75.
6. Jaattela,M. (2004) Multiple cell death pathways as regulators of tumour initiation and progression. *Oncogene*, **23**, 2746–2756.
7. Plas,D.R. and Thompson,C.B. (2002) Cell metabolism in the regulation of programmed cell death. *Trends Endocrinol. Metab.*, **13**, 75–78.
8. Danial,N.N., Gramm,C.F., Scorrano,L. *et al.* (2003) BAD and glucokinase reside in a mitochondrial complex that integrates glycolysis and apoptosis. *Nature*, **424**, 952–956.
9. Azoulay-Zohar,H., Israelson,A., Abu-Hamad,S. and Shoshan-Barmatz,V. (2004) In self-defence: hexokinase promotes voltage-dependent anion channel closure and prevents mitochondria-mediated apoptotic cell death. *Biochem. J.*, **377**, 347–355.
10. Vahsen,N., Cande,C., Briere,J.J. *et al.* (2004) AIF deficiency compromises oxidative phosphorylation. *EMBO J.*, **23**, 4679–4689.
11. Jacobson,M.D., Burne,J.F., King,M.P., Miyashita,T., Reed,J.C. and Raff,M.C. (1993) Bcl-2 blocks apoptosis in cells lacking mitochondrial DNA. *Nature*, **361**, 365–369.
12. Marchetti,P., Susin,S.A., Decaudin,D., Gamen,S., Castedo,M., Hirsch,T., Zamzami,N., Naval,J., Senik,A. and Kroemer,G. (1996) Apoptosis-associated derangement of mitochondrial function in cells lacking mitochondrial DNA. *Cancer Res.*, **56**, 2033–2038.
13. Jiang,S., Cai,J., Wallace,D.C. and Jones,D.P. (1999) Cytochrome *c*-mediated apoptosis in cells lacking mitochondrial DNA. Signaling pathway involving release and caspase 3 activation is conserved. *J. Biol. Chem.*, **274**, 29905–29911.
14. Dey,R. and Moraes,C.T. (2000) Lack of oxidative phosphorylation and low mitochondrial membrane potential decrease susceptibility to apoptosis and do not modulate the protective effect of Bcl-x(L) in osteosarcoma cells. *J. Biol. Chem.*, **275**, 7087–7094.
15. Kim,J.Y., Kim,Y.H., Chang,I., Kim,S., Pak,Y.K., Oh,B.H., Yagita,H., Jung,Y.K., Oh,Y.J. and Lee,M.S. (2002) Resistance of mitochondrial DNA-deficient cells to TRAIL: role of Bax in TRAIL-induced apoptosis. *Oncogene*, **21**, 3139–3148.
16. Park,S.Y., Chang,I., Kim,J.Y., Kang,S.W., Park,S.H., Singh,K. and Lee,M.S. (2004) Resistance of mitochondrial DNA-depleted cells against cell death: role of mitochondrial superoxide dismutase. *J. Biol. Chem.*, **279**, 7512–7520.
17. Wolvetang,E.J., Johnson,K.L., Krauer,K., Ralph,S.J. and Linnane,A.W. (1994) Mitochondrial respiratory chain inhibitors induce apoptosis. *FEBS Lett.*, **339**, 40–44.
18. Peachman,K.K., Lyles,D.S. and Bass,D.A. (2001) Mitochondria in eosinophils: functional role in apoptosis but not respiration. *Proc. Natl Acad. Sci. USA*, **98**, 1717–1722.
19. Matsuyama,S., Xu,Q., Velours,J. and Reed,J.C. (1998) The Mitochondrial F0F1-ATPase proton pump is required for function of the proapoptotic protein Bax in yeast and mammalian cells. *Mol. Cell*, **1**, 327–336.
20. Shchepina,L.A., Pletjushkina,O.Y., Avetisyan,A.V., Bakeeva,L.E., Fetisova,E.K., Izyumov,D.S., Saprunova,V.B., Vyssokikh,M.Y., Chernyak,B.V. and Skulachev,V.P. (2002) Oligomycin, inhibitor of the F0 part of H+-ATP-synthase, suppresses the TNF-induced apoptosis. *Oncogene*, **21**, 8149–8157.
21. Harris,M.H., Vander Heiden,M.G., Kron,S.J. and Thompson,C.B. (2000) Role of oxidative phosphorylation in Bax toxicity. *Mol. Cell. Biol.*, **20**, 3590–3596.
22. Gross,A., Pilcher,K., Blachly-Dyson,E., Basso,E., Jockel,J., Bassik,M.C., Korsmeyer,S.J. and Forte,M. (2000) Biochemical and genetic analysis of

the mitochondrial response of yeast to BAX and BCL-X(L). *Mol. Cell. Biol.*, **20**, 3125–3136.
23. López de Heredia,M., Izquierdo,J.M. and Cuezva,J.M. (2000) A conserved mechanism for controlling the translation of beta-F1-ATPase mRNA between the fetal liver and cancer cells. *J. Biol. Chem.*, **275**, 7430–7437.
24. Cuezva,J.M., Krajewska,M., de Heredia,M.L., Krajewski,S., Santamaria,G., Kim,H., Zapata,J.M., Marusawa,H., Chamorro,M. and Reed,J.C. (2002) The bioenergetic signature of cancer: a marker of tumor progression. *Cancer Res.*, **62**, 6674–6681.
25. Isidoro,A., Martinez,M., Fernandez,P.L., Ortega,A.D., Santamaria,G., Chamorro,M., Reed,J.C. and Cuezva,J.M. (2004) Alteration of the bioenergetic phenotype of mitochondria is a hallmark of breast, gastric, lung and oesophageal cancer. *Biochem. J.*, **378**, 17–20.
26. Cuezva,J.M., Chen,G., Alonso,A.M., Isidoro,A., Misek,D.E., Hanash,S.M. and Beer,D.G. (2004) The bioenergetic signature of lung adenocarcinomas is a molecular marker of cancer diagnosis and prognosis. *Carcinogenesis*, **25**, 1157–1163.
27. Unwin,R.D., Craven,R.A., Harnden,P., Hanrahan,S., Totty,N., Knowles,M., Eardley,I., Selby,P.J. and Banks,R.E. (2003) Proteomic changes in renal cancer and co-ordinate demonstration of both the glycolytic and mitochondrial aspects of the Warburg effect. *Proteomics*, **3**, 1620–1632.
28. Meierhofer,D., Mayr,J.A., Foetschl,U., Berger,A., Fink,K., Schmeller,N., Hacker,G.W., Hauser-Kronberger,C., Kofler,B. and Sperl,W. (2004) Decrease of mitochondrial DNA content and energy metabolism in renal cell carcinomas. *Carcinogenesis*, **25**, 1005–1010.
29. Yin,P.H., Lee,H.C., Chau,G.Y., Wu,Y.T., Li,S.H., Lui,W.Y., Wei,Y.H., Liu,T.Y. and Chi,C.W. (2004) Alteration of the copy number and deletion of mitochondrial DNA in human hepatocellular carcinoma. *Br. J. Cancer*, **90**, 2390–2396.
30. He,Q.Y., Chen,J., Kung,H.F., Yuen,A.P. and Chiu,J.F. (2004) Identification of tumor-associated proteins in oral tongue squamous cell carcinoma by proteomics. *Proteomics*, **4**, 271–278.
31. Shin,Y.K., Yoo,B.C., Chang,H.J., Jeon,E., Hong,S.H., Jung,M.S., Lim,S.J. and Park,J.G. (2005) Down-regulation of mitochondrial F1F0-ATP synthase in human colon cancer cells with induced 5-fluorouracil resistance. *Cancer Res.*, **65**, 3162–3170.
32. Di Liegro,C.M., Bellafiore,M., Izquierdo,J.M., Rantanen,A. and Cuezva,J.M. (2000) 3′-Untranslated regions of oxidative phosphorylation mRNAs function *in vivo* as enhancers of translation. *Biochem. J.*, **352**, 109–115.
33. Herrera,B., Fernandez,M., Alvarez,A.M., Roncero,C., Benito,M., Gil,J. and Fabregat,I. (2001) Activation of caspases occurs downstream from radical oxygen species production, Bcl-xL down-regulation, and early cytochrome *c* release in apoptosis induced by transforming growth factor beta in rat fetal hepatocytes. *Hepatology*, **34**, 548–556.
34. Herrera,B., Alvarez,A.M., Sanchez,A., Fernandez,M., Roncero,C., Benito,M. and Fabregat,I. (2001) Reactive oxygen species (ROS) mediates the mitochondrial-dependent apoptosis induced by transforming growth factor (beta) in fetal hepatocytes. *FASEB J.*, **15**, 741–751.
35. Matsuyama,S., Llopis,J., Deveraux,Q.L., Tsien,R.Y. and Reed,J.C. (2000) Changes in intramitochondrial and cytosolic pH: early events that modulate caspase activation during apoptosis. *Nat. Cell. Biol.*, **2**, 318–325.
36. Bowman,E.J., Siebers,A. and Altendorf,K. (1988) Bafilomycins: a class of inhibitors of membrane ATPases from microorganisms, animal cells, and plant cells. *Proc. Natl Acad. Sci. USA*, **85**, 7972–7976.
37. Mathiasen,I.S. and Jaattela,M. (2002) Triggering caspase-independent cell death to combat cancer. *Trends Mol. Med.*, **8**, 212–220.
38. Mattson,M.P. and Kroemer,G. (2003) Mitochondria in cell death: novel targets for neuroprotection and cardioprotection. *Trends Mol. Med.*, **9**, 196–205.
39. Karawajew,L., Rhein,P., Czerwony,G. and Ludwig,W.D. (2005) Stress-induced activation of the p53 tumor suppressor in leukemia cells and normal lymphocytes requires mitochondrial activity and reactive oxygen species. *Blood*, **105**, 4767–4775.
40. von Ahsen,O., Renken,C., Perkins,G., Kluck,R.M., Bossy-Wetzel,E. and Newmeyer,D.D. (2000) Preservation of mitochondrial structure and function after Bid- or Bax-mediated cytochrome *c* release. *J. Cell. Biol.*, **150**, 1027–1036.
41. Frank,S., Gaume,B., Bergmann-Leitner,E.S., Leitner,W.W., Robert,E.G., Catez,F., Smith,C.L. and Youle,R.J. (2001) The role of dynamin-related protein 1, a mediator of mitochondrial fission, in apoptosis. *Dev. Cell*, **1**, 515–525.
42. Jagasia,R., Grote,P., Westermann,B. and Conradt,B. (2005) DRP-1-mediated mitochondrial fragmentation during EGL-1-induced cell death in *C. elegans*. *Nature*, **433**, 754–760.
43. Perfettini,J.L., Roumier,T. and Kroemer,G. (2005) Mitochondrial fusion and fission in the control of apoptosis. *Trends Cell. Biol.*, **15**, 179–183.
44. Scarlett,J.L., Sheard,P.W., Hughes,G., Ledgerwood,E.C., Ku,H.H. and Murphy,M.P. (2000) Changes in mitochondrial membrane potential during staurosporine-induced apoptosis in Jurkat cells. *FEBS Lett*, **475**, 267–272.
45. Rego,A.C., Vesce,S. and Nicholls,D.G. (2001) The mechanism of mitochondrial membrane potential retention following release of cytochrome *c* in apoptotic GT1-7 neural cells. *Cell Death Differ.*, **8**, 995–1003.
46. Buchet,K. and Godinot,C. (1998) Functional F1-ATPase essential in maintaining growth and membrane potential of human mitochondrial DNA-depleted rho degrees cells. *J. Biol. Chem.*, **273**, 22983–22989.
47. Nicholls,D.G. and Ward,M.W. (2000) Mitochondrial membrane potential and neuronal glutamate excitotoxicity: mortality and millivolts. *Trends Neurosci.*, **23**, 166–174.
48. Almeida,A., Almeida,J., Bolanos,J.P. and Moncada,S. (2001) Different responses of astrocytes and neurons to nitric oxide: the role of glycolytically generated ATP in astrocyte protection. *Proc. Natl Acad. Sci. USA*, **98**, 15294–15299.
49. Votyakova,T.V. and Reynolds,I.J. (2001) DeltaPsi(m)-Dependent and independent production of reactive oxygen species by rat brain mitochondria. *J. Neurochem*, **79**, 266–277.
50. Brand,M.D., Affourtit,C., Esteves,T.C., Green,K., Lambert,A.J., Miwa,S., Pakay,J.L. and Parker,N. (2004) Mitochondrial superoxide: production, biological effects, and activation of uncoupling proteins. *Free Radic. Biol. Med.*, **37**, 755–767.
51. Lambert,A.J. and Brand,M.D. (2004) Superoxide production by NADH:ubiquinone oxidoreductase (complex I) depends on the pH gradient across the mitochondrial inner membrane. *Biochem. J.*, **382**, 511–517.
52. Chandra,J., Samali,A. and Orrenius,S. (2000) Triggering and modulation of apoptosis by oxidative stress. *Free Radic. Biol. Med.*, **29**, 323–333.
53. Martinvalet,D., Zhu,P. and Lieberman,J. (2005) Granzyme A induces caspase-independent mitochondrial damage, a required first step for apoptosis. *Immunity*, **22**, 355–370.
54. Klaunig,J.E. and Kamendulis,L.M. (2004) The role of oxidative stress in carcinogenesis. *Annu. Rev. Pharmacol. Toxicol*, **44**, 239–267.
55. Ricci,J.E., Munoz-Pinedo,C., Fitzgerald,P., Bailly-Maitre,B., Perkins,G.A., Yadava,N., Scheffler,I.E., Ellisman,M.H. and Green,D.R. (2004) Disruption of mitochondrial function during apoptosis is mediated by caspase cleavage of the p75 subunit of complex I of the electron transport chain. *Cell*, **117**, 773–786.
56. Miramar,M.D., Costantini,P., Ravagnan,L., Saraiva,L.M., Haouzi,D., Brothers,G., Penninger,J.M., Peleato,M.L., Kroemer,G. and Susin,S.A. (2001) NADH oxidase activity of mitochondrial apoptosis-inducing factor. *J. Biol. Chem.*, **276**, 16391–16398.
57. Lee,S.S., Lee,R.Y., Fraser,A.G., Kamath,R.S., Ahringer,J. and Ruvkun,G. (2003) A systematic RNAi screen identifies a critical role for mitochondria in *C. elegans* longevity. *Nat. Genet.*, **33**, 40–48.

Received November 15, 2005; revised December 1, 2005; accepted December 13, 2005